

Supplementary Information

Layer-by-layer assembled superhydrophobic composite aerogel for rapid and high-capacity removal of microplastics from beverages

Qiyue Zhao^a, Xingxu Jiang^b, Ergen Bao^c Hong-Man Hou^a, Gong-Liang Zhang^a, Jingran Bi^{a}*

^a SKL of Marine Food Processing & Safety Control, National Engineering Research Center of Seafood, Collaborative Innovation Center of Seafood Deep Processing, Liaoning Key Lab for Aquatic Processing Quality and Safety, School of Food Science and Technology, Dalian Polytechnic University, Dalian 116034, China.

^b School of Materials Science and Engineering, Beihang University, Beijing, 100191, China.

^c School of Materials Science and Engineering, Northeastern University, Shenyang, 110819, China.

* Corresponding author
E-mail address: bijingran1225@foxmail.com (J. Bi).

1. Experimental method

1.1 Determination of in vitro cytotoxicity

In vitro cytotoxicity assay was performed using CCK-8 assay. Sterilized AG, AG^{U6-(OH)2} and AG^{U6-(OH)2}@PMSQ (20 mg) were soaked in 1 mL of Dulbecco's Modified Eagle's Medium (DMEM) and incubated for 24 h at 37 °C to obtain extract for sample determination. GES-1 and intestinal mucosal epithelial cells were inoculated in 96-well plates at a density of 5000 cells per well and incubated for 48 h (37 °C, 5% CO₂). The culture medium (DMEM) was replaced by 200 µL of basal medium with AG, AG^{U6-(OH)2} and AG^{U6-(OH)2}@PMSQ. The extract-free basal medium was used as the blank control.

CCK8 assay: The medium was replaced with 180 µL of DMEM and 20 µL of CCK-8 (HY-K0301, MCE, USA) and incubated for another 2 h. The absorbance was assayed at a wavelength of 450 nm. Cell viability was reflected as the percentage of absorbance relative to that of the untreated control. Three individual experiments were performed and analyzed in each group.

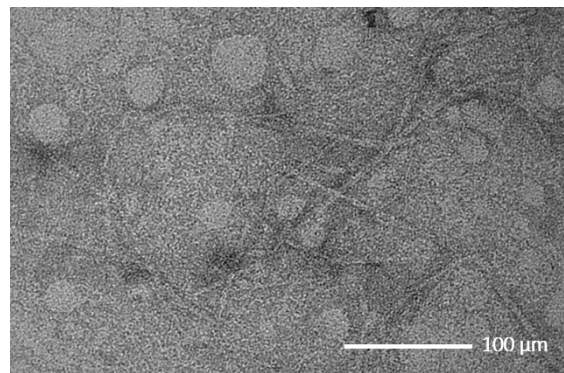


Fig. S1. TEM images of CNFs.

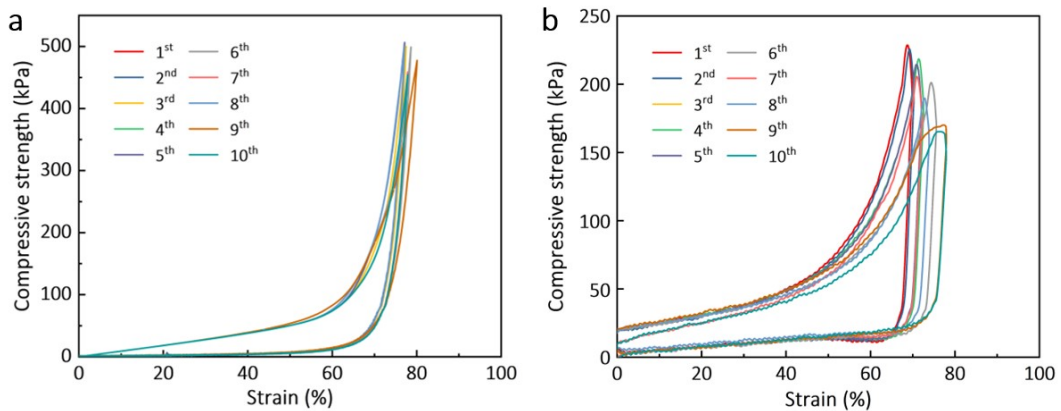


Fig. S2. Ten compressive stress-strain cycle curves for (a) AG and (b) aerogels with single CNFs network in the wet state (70 % compressive strain).

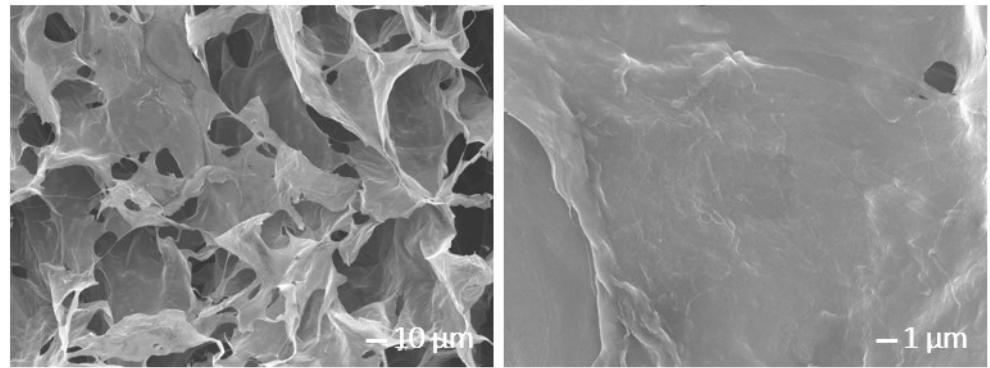


Fig. S3. SEM images of AG at different scales.

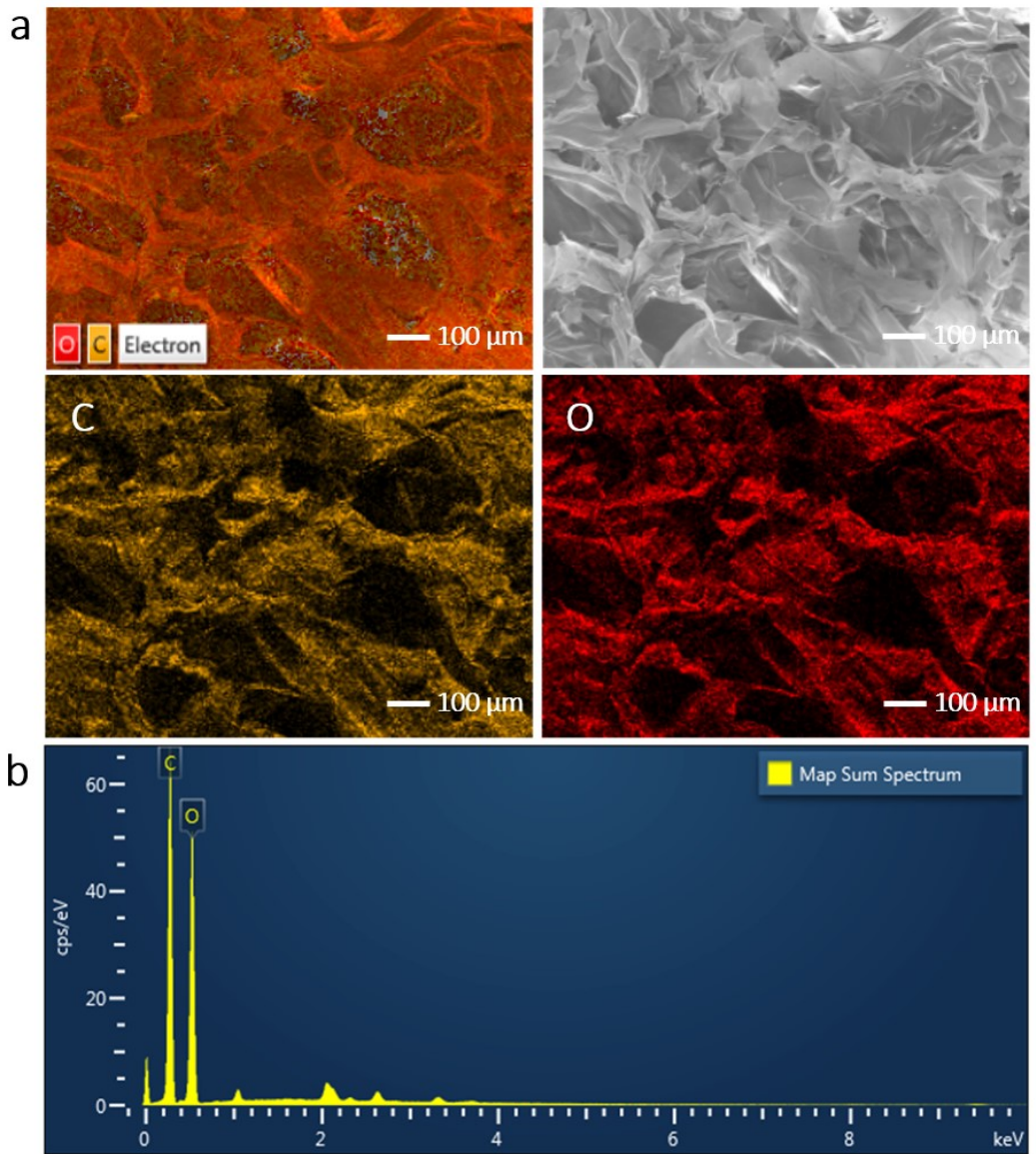


Fig. S4. (a) EDS maps and (b) spectrum of the detected elements in the analyzed region of the SEM image for AG.

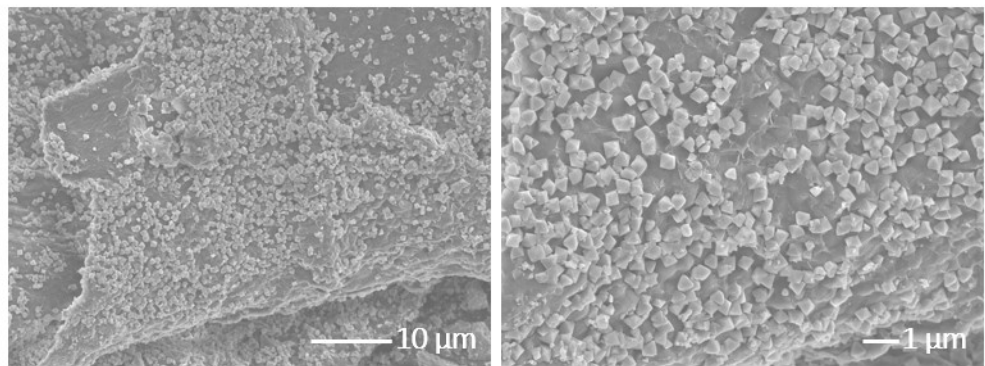


Fig. S5. SEM images of $\text{AG}^{\text{U6-(OH)}_2}$ at different scales.

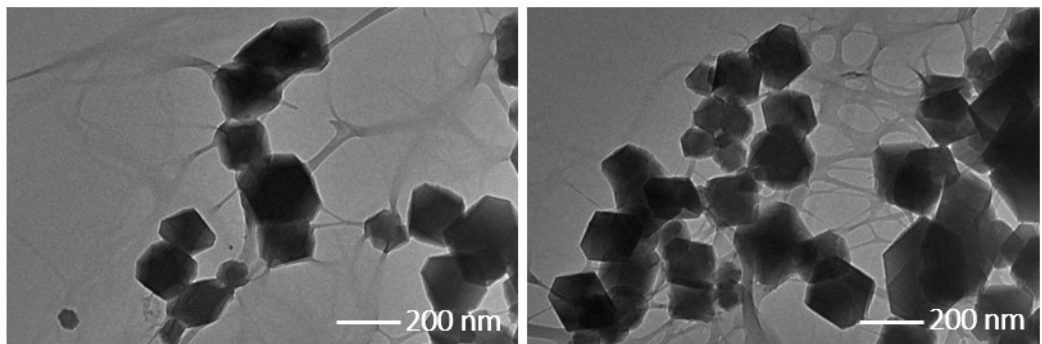


Fig. S6. TEM images of $\text{AG}^{\text{U6-(OH)}_2}$.

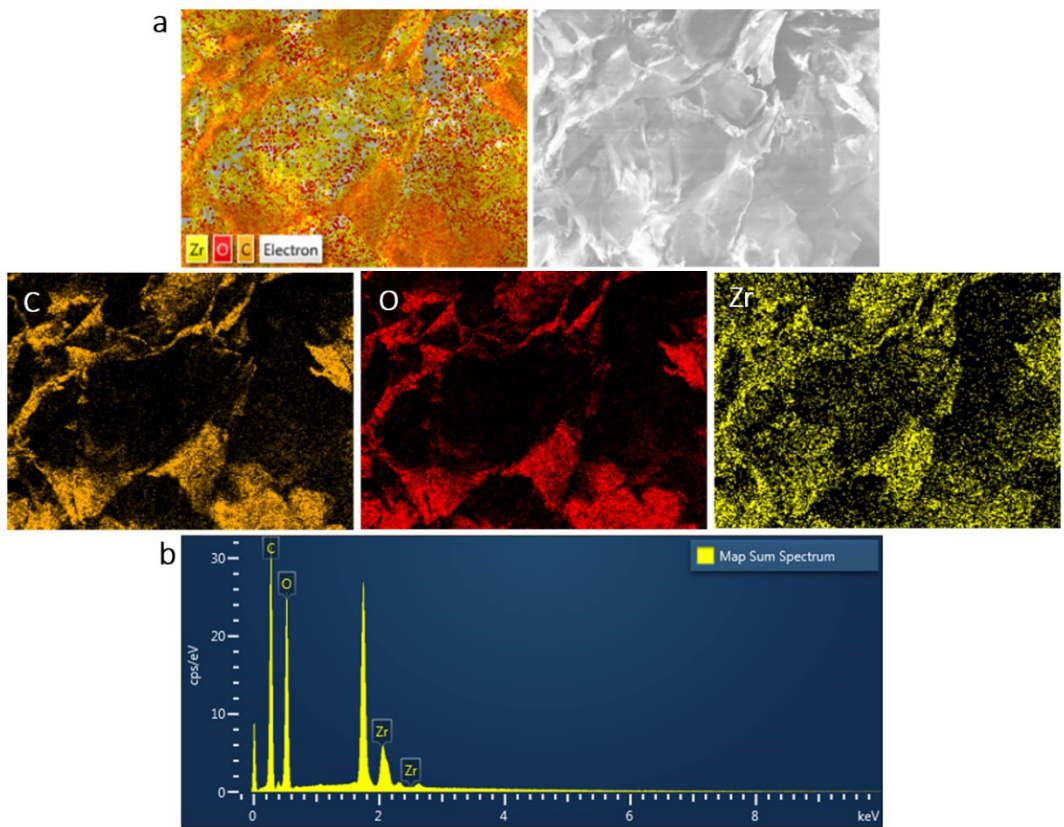


Fig. S7. (a) EDS maps and (b) spectrum of the detected elements in the analyzed region of the SEM image for $\text{AG}^{\text{U6-(OH)}_2}$.

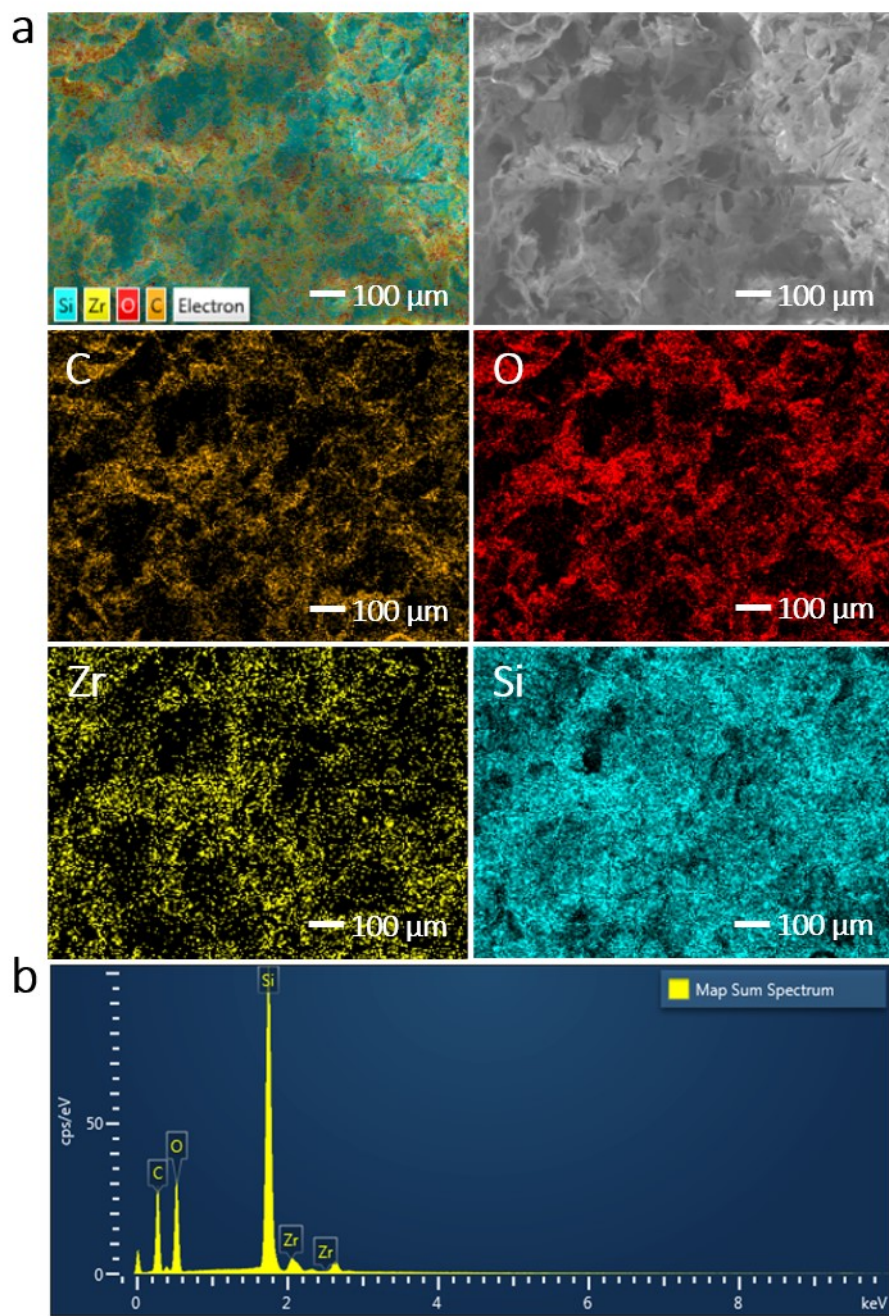


Fig. S8. (a) EDS maps and (b) spectrum of the detected elements in the analyzed region of the SEM image for $\text{AG}^{\text{U}6\text{-(OH)}_2}\text{@PMSQ}$

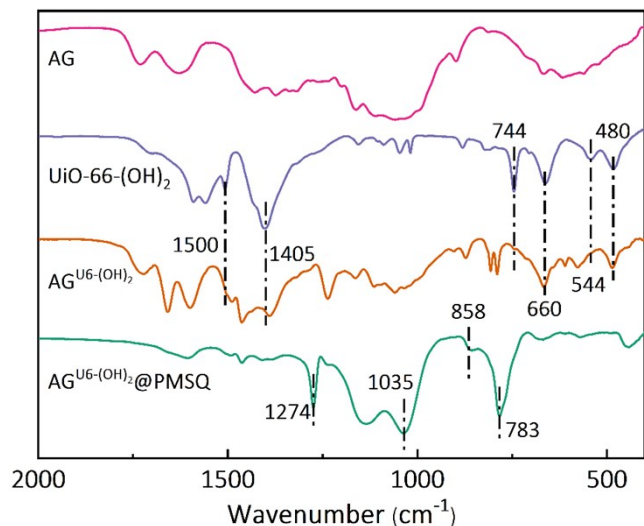


Fig. S9. The FT-IR spectra (450-2000 cm⁻¹) of AG, AG^{U6-(OH)2}, and AG^{U6-(OH)2}@PMSQ

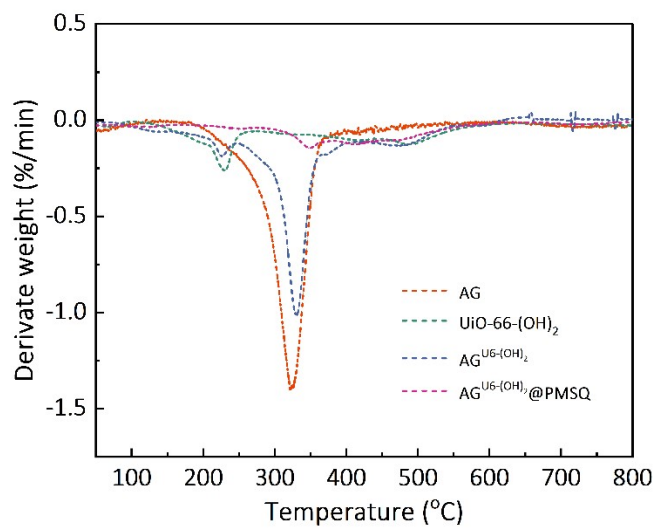


Fig. S10. The DTG curves of AG, UiO-66-(OH)₂, AG^{U6-(OH)2}, and AG^{U6-(OH)2}@PMSQ

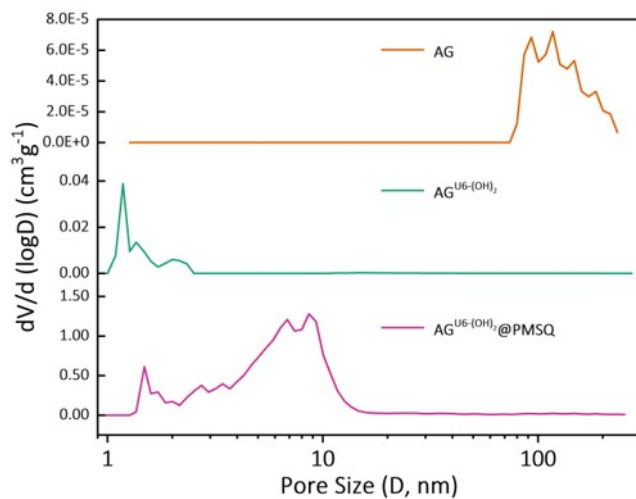


Fig. S11. DFT pore size distributions of AG, $\text{AG}^{\text{U6-(OH)}_2}$ and $\text{AG}^{\text{U6-(OH)}_2}\text{@PMSQ}$

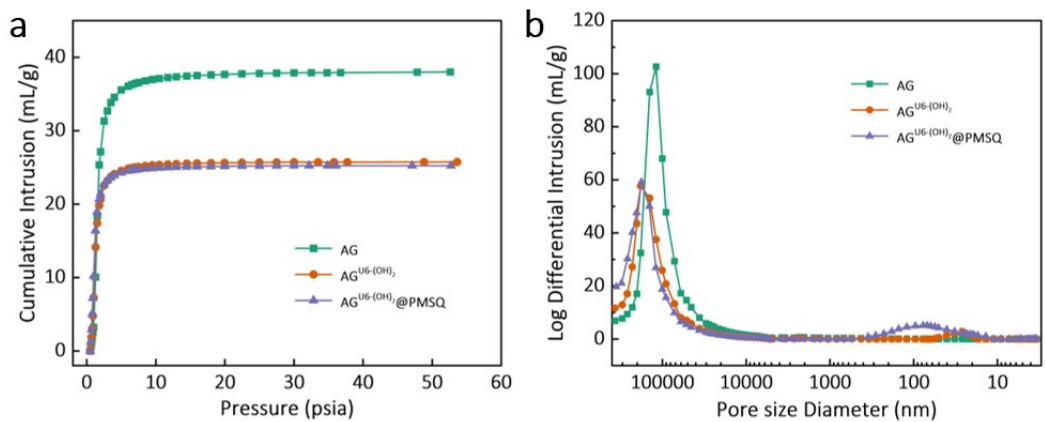


Fig. S12. (a) Mercury intrusion curves and (b) pore size distribution of AG, AG^{U6-(OH)₂} and AG^{U6-(OH)₂}@PMSQ

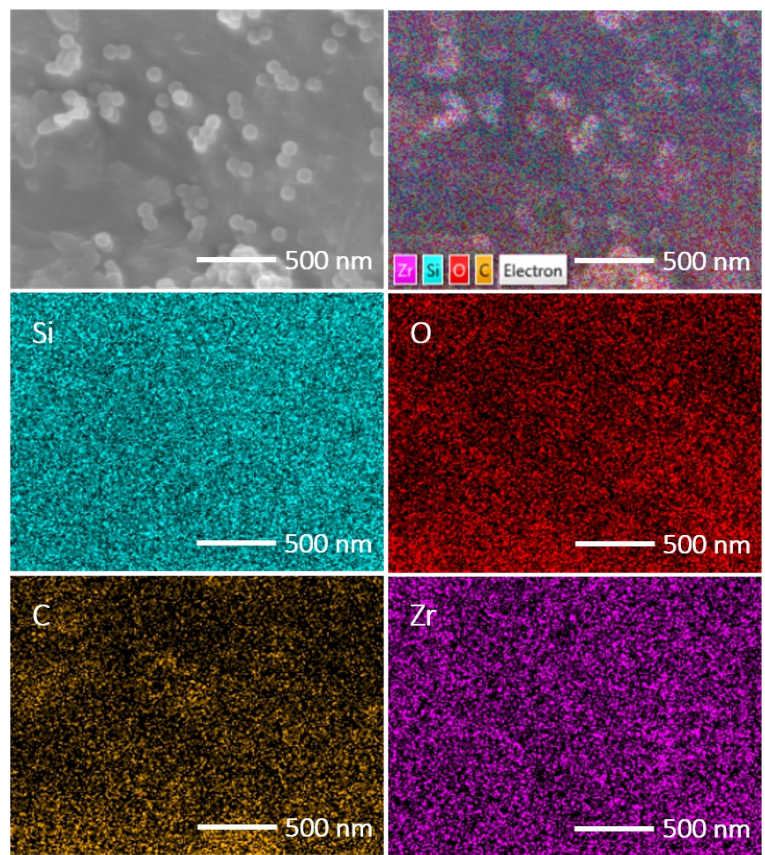


Fig. S13. SEM and EDS spectra of PSM adsorbed by $\text{AGU}^{6-(\text{OH})_2}@\text{PMSQ}$

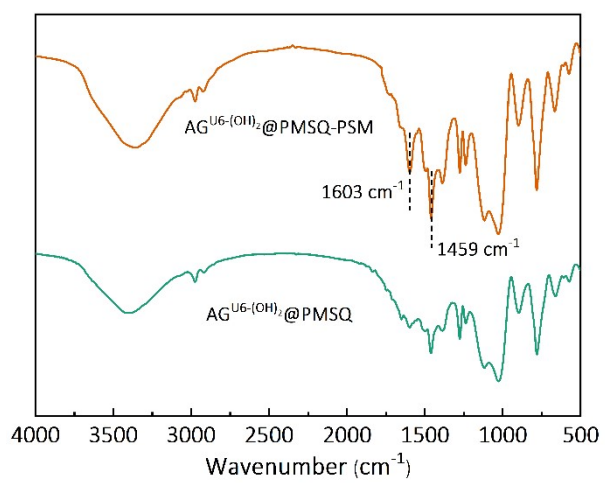


Fig. S14. FT-IR spectra before and after PSM adsorption by $\text{AG}^{\text{U6-(OH)}_2}@\text{PMSQ}$

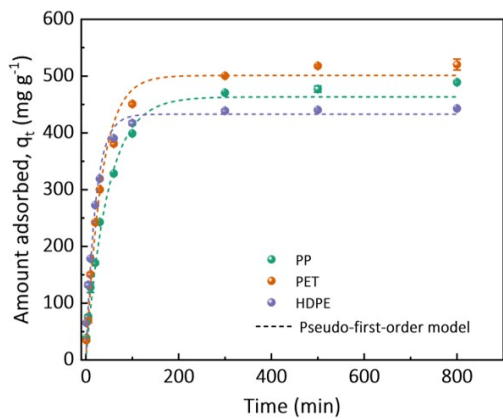


Fig. S15. Adsorption capacity of AGU6-(OH)₂@PMSQ on PP, PET and HDPE

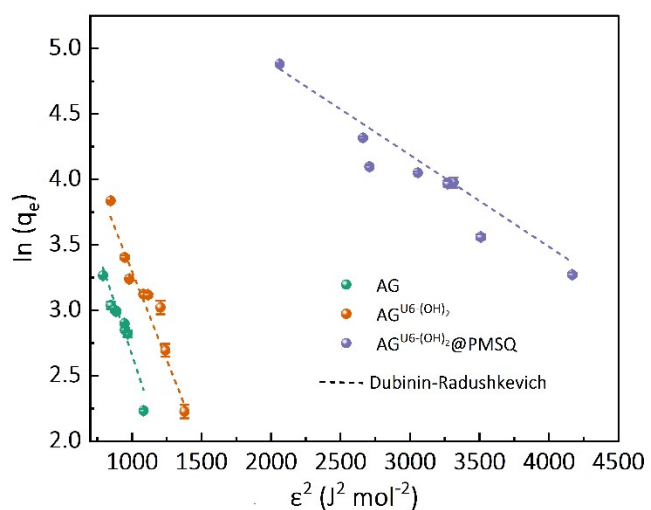


Fig. S16. The fitting of D-R of AG, $\text{AG}^{U6-(OH)_2}$, and $\text{AG}^{U6-(OH)_2}@\text{PMSQ}$ for PSM

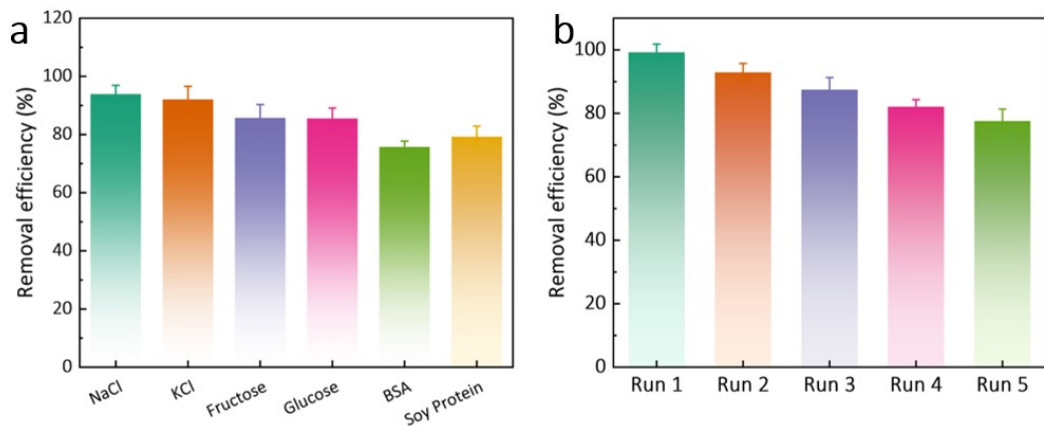


Fig. S17. (a) Removal efficiency of $\text{AG}^{\text{U}6\text{-(OH)}_2}\text{@PMSQ}$ for PSM in different interference environments. (d) The recyclability of $\text{AG}^{\text{U}6\text{-(OH)}_2}\text{@PMSQ}$ for the adsorption of PSM

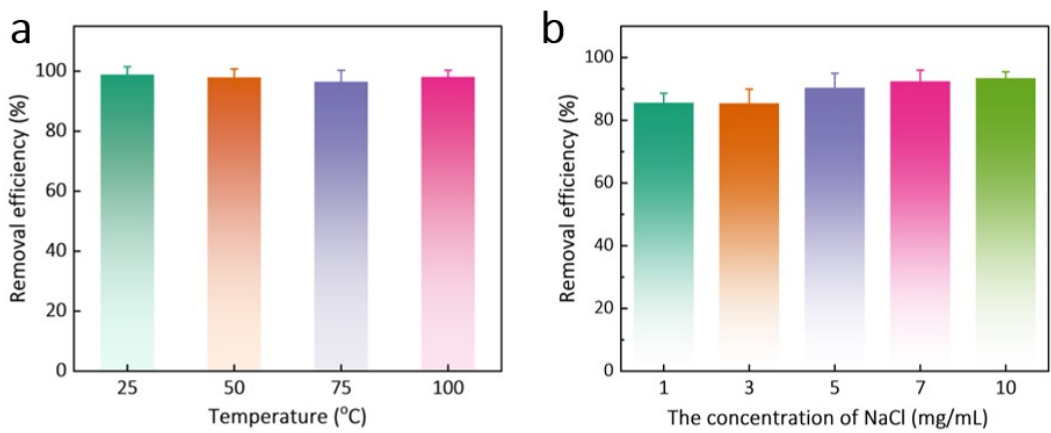


Fig. S18. Removal efficiency of $\text{AG}^{\text{U6}-\text{(OH})_2}\text{@PMSQ}$ for PSM at different temperatures and ionic strengths

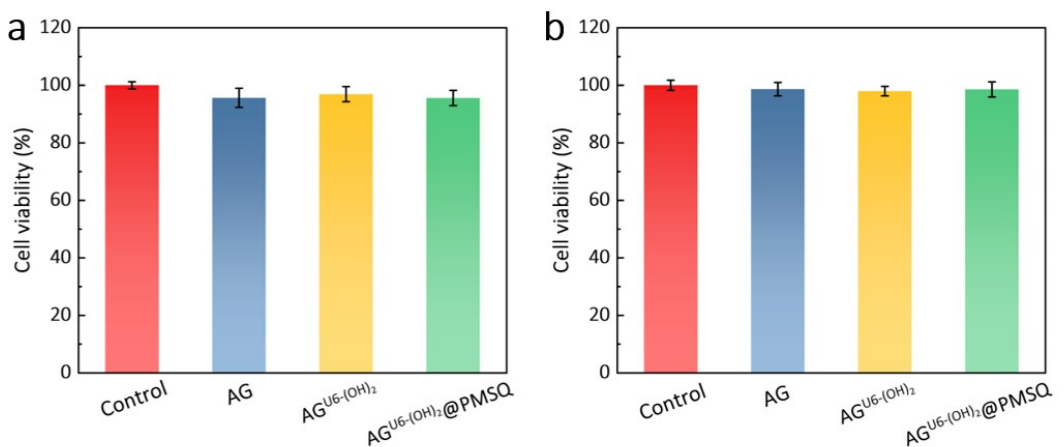


Fig. S19. Cell viability of GES-1 and intestinal mucosal epithelial cells in AG, $\text{AG}^{\text{U6-(OH)}_2}$, and $\text{AG}^{\text{U6-(OH)}_2}@\text{PMSQ}$

Table S1. Elementary composition analysis of AG, AG^{U6-(OH)2} and AG^{U6-(OH)2@PMSQ}

Element	AG (wt%)	AG ^{U6-(OH)2} (wt%)	AG ^{U6-(OH)2@PMSQ} (wt%)	AG ^{U6-(OH)2@PMSQ with PSM} (wt%)
C	49.16	49.90	46.50	53.36
O	50.84	41.65	27.32	30.58
Zr		8.45	3.35	2.06
Si			22.84	14.00
Total	100	100	100	100

Table S2. Specific surface areas and cumulative surface area of AG, AG^{U6-(OH)₂} and AG^{U6-(OH)₂}@PMSQ

Samples	S _{BET} (m ² /g)	cumulative surface area (m ² /g)			<i>V_{Mi}</i> (%) ^a	<i>V_{Me}</i> (%) ^b	<i>V_{Ma}</i> (%) ^c
		Micropores (< 2 nm)	Mesopores (2 nm-50 nm)	Macropores (> 50 nm)			
AG	4.02	0.00	0.0017	0.0061	0.00%	29.07%	70.93%
AG ^{U6-(OH)₂}	194.24	29.46	8.37	8.76	63.23%	17.97%	18.80%
AG ^{U6-(OH)₂} @PMSQ	449.19	58.38	188.27	2.21	23.46%	75.65%	0.89%

^a: *V_{Mi}* is the percentage of micropores in the total pore volume

^b: *V_{Me}* is the percentage of mesopores in the total pore volume

^c: *V_{Ma}* is the percentage of macropores in the total pore volume

Table S3. Comparisons of adsorption capacity of $\text{AG}^{\text{U6-(OH)}_2}@\text{PMSQ}$ with previously reported cellulose-based adsorbents.

Materials	Water contact angle (°)	Absorption capacity of chloroform (g/g)	Ref.
Silylated nanocellulose sponge	136	102	1
Modified cellulose nanofibrils (CNF) aerogel	149	46.6	2
Silylated wood sponge	151	41	3
EVOH/ Al_2O_3 aerogel	160.8	64.9	4
$\text{AG}^{\text{U6-(OH)}_2}@\text{PMSQ}$	157.1	104	This work

Table S4. Comparison of AG^{U6-(OH)2}@PMSQ with other adsorbents for PSM

Materials	Equilibrium time (h)	Ref
Starch-gelatin sponge	22	5
M-CNTs	2	6
ChGO	10	7
ChGO-CT	12	8
NPs/MPs	10	9
AG ^{U6-(OH)2} @PMSQ	1.67	This work

Table S5. Pseudo-first-order kinetic parameters for PSM on AG, AG^{U6-(OH)2} and AG^{U6-(OH)2}@PMSQ

Samples	AG			AG ^{U6-(OH)2}			AG ^{U6-(OH)2} @PMSQ		
	q_e (mg/g)	k_1 (min ⁻¹)	R ²	q_e (mg/g)	k_1 (min ⁻¹)	R ²	q_e (mg/g)	k_1 (min ⁻¹)	R ²
PSM	357.852	0.031	0.8962	390.140	0.032	0.9242	525.322	0.038	0.9711

Table S6. Pseudo-second-order kinetic parameters for PSM on AG, AG^{U6-(OH)₂} and AG^{U6-(OH)₂}@PMSQ

Samples	AG			AG ^{U6-(OH)₂}			AG ^{U6-(OH)₂} @PMSQ		
	q_e (mg/g)	k_2 (min ⁻¹)	R ²	q_e (mg/g)	k_2 (min ⁻¹)	R ²	q_e (mg/g)	k_2 (min ⁻¹)	R ²
PSM	384.615	1.351e ⁻⁷	0.9968	434.783	3.375e ⁻⁷	0.9980	555.556	3.961e ⁻⁷	0.9976

Table S7. Comparison of maximum adsorption capacity of adsorbents for PSM removal

Materials	q_e (mg/g)	Ref
PEI-CNFs	150.75	¹⁰
M2A500	215.58	¹¹
CPEA	146.38	¹²
G@LDO700	212.77	¹³
LS-B (2)	381.68	¹⁴
$\text{AG}^{\text{U6-(OH)}_2}\text{@PMSQ}$	555.56	This work

Table S8. Pseudo-first-order kinetic parameters for PP, PET, and HDPE on AG^{U6-(OH)2}@PMSQ

	q_e (mg/g)	k_1 (min ⁻¹)	R^2
PP	463.26	0.021	0.9818
PET	501.10	0.030	0.9885
HDPE	432.89	0.048	0.9786

Table S9. Intraparticle diffusion kinetic parameters for PSM on AG, AG^{U6-(OH)2} and AG^{U6-(OH)2}@PMSQ

	AG			AG ^{U6-(OH)2}			AG ^{U6-(OH)2} @PMSQ		
	k_i (mg/g·min ^{1/2})	C_i (mg/g)	R ²	k_i (mg/g·min ^{1/2})	C_i (mg/g)	R ²	k_i (mg/g·min ^{1/2})	C_i (mg/g)	R ²
The first phase	26.010	63.376	0.9075	54.637	-45.441	0.9173	56.760	9.611	0.9965
The second phase	9.782	183.310	0.7984	9.988	208.050	0.9980	/	/	/
The third phase	4.465	261.110	0.9821	4.118	307.960	0.9934	3.945	446.660	0.8634

Table S10. Parameters of Langmuir adsorption isotherm models for PSM on AG, AG^{U6-(OH)₂} and AG^{U6-(OH)₂}@PMSQ

Samples	AG			AG ^{U6-(OH)₂}			AG ^{U6-(OH)₂} @PMSQ		
	q_{\max}	k_L	R^2	q_{\max}	k_L	R^2	q_{\max}	k_L	R^2
	(mg/g)	(L/mg)		(mg/g)	(L/mg)		(mg/g)	(L/mg)	
PSM	1428.571	0.003	0.1343	-833.333	-0.005	0.2791	1428.571	0.001	0.7728

Table S11. Parameters of Freundlich adsorption isotherm models for PSM on AG, AG^{U6-(OH)2} and AG^{U6-(OH)2}@PMSQ

Samples	AG			AG ^{U6-(OH)2}			AG ^{U6-(OH)2} @PMSQ		
	k_F (mg ^{1-1/n} L ^{1/n} /g)	1/n	R ²	k_F (mg ^{1-1/n} L ^{1/n} /g)	1/n	R ²	k_F (mg ^{1-1/n} L ^{1/n} /g)	1/n	R ²
PSM	43.410	0.214	0.9098	30.753	0.290	0.8235	1.969	0.773	0.9613

Table S12. Parameters of D-R adsorption isotherm models for PSM on AG, $\text{AG}^{\text{U6-(OH)}2}$, and $\text{AG}^{\text{U6-(OH)}2}@\text{PMSQ}$

Samples	AG	$\text{AG}^{\text{U6-(OH)}2}$	$\text{AG}^{\text{U6-(OH)}2}@PMSQ$
K_{DR} (mol ² kJ ⁻²)	0.0013	0.0014	0.0007
Q_{MAX} (mg/g)	350.16	402.09	536.70
E (kJ mol ⁻¹)	19.61	18.90	26.73
R ²	0.9451	0.9687	0.9583

Table S13. Calibration curves and LOD, LOQ of PSM

Samples	Liner range (mg/mL)	Calibration	R ²	LOD (µg/mL)	LOQ (µg/mL)
Deionized water	1-10	$Y = 15369x + 4633.7$	0.9999	0.13	0.43
Bottle water	1-10	$Y = 15388x + 4592.4$	0.9997	0.12	0.4
Gatorade	1-10	$Y = 15844x + 4296.0$	0.9993	0.22	0.73
Soda drink	1-10	$Y = 15039x + 4835.7$	0.9996	0.16	0.53
Sprite	1-10	$Y = 15128x + 4373.1$	0.9990	0.21	0.70
Coffee	1-10	$Y = 15663x + 4941.6$	0.9976	0.29	0.97
Tea	1-10	$Y = 15534x + 4132.0$	0.9989	0.18	0.60

Table S14. Simulation results of PSM molecules on PMSQ surface

Components'	E_{all} (kcal/mol)	$E_{surface}$ (kcal/mol)	$E_{adsorbate}$ (kcal/mol)	E_{ads} (kcal/mol)
PSM	-390.59	-260.90	-125.63	-4.06

1. Z. Zhang, G. Sèbe, D. Rentsch, T. Zimmermann and P. Tingaut, *Chemistry of Materials*, 2014, **26**, 2659-2668.
2. A. Mulyadi, Z. Zhang and Y. Deng, *ACS Applied Materials & Interfaces*, 2016, **8**, 2732-2740.
3. H. Guan, Z. Cheng and X. Wang, *ACS Nano*, 2018, **12**, 10365-10373.
4. J. Lu, Y. Li, W. Song, M. D. Losego, R. Monikandan, K. I. Jacob and R. Xiao, *ACS Nano*, 2020, **14**, 7999-8011.
5. J. Fu, N. Liu, Y. Peng, G. Wang, X. Wang, Q. Wang, M. Lv and L. Chen, *Journal of Hazardous Materials*, 2023, **456**, 131685.
6. Y. Tang, S. Zhang, Y. Su, D. Wu, Y. Zhao and B. Xie, *Chemical Engineering Journal*, 2021, **406**, 126804.
7. C. Sun, Z. Wang, L. Chen and F. Li, *Chemical Engineering Journal*, 2020, **393**, 124796.
8. C. Sun, Z. Wang, H. Zheng, L. Chen and F. Li, *Journal of Hazardous Materials*, 2021, **420**, 126599.
9. H. Zhao, X. Huang, L. Wang, X. Zhao, F. Yan, Y. Yang, G. Li, P. Gao and P. Ji, *Chemical Engineering Journal*, 2022, **430**, 133122.
10. J. Zhuang, M. Pan, Y. Zhang, F. Liu and Z. Xu, *International Journal of Biological Macromolecules*, 2023, **235**, 123884.
11. X. Li, W. Liu, J. Zhang, Z. Wang, Z. Guo, J. Ali, L. Wang, Z. Yu, X. Zhang and Y. Sun, *Chemosphere*, 2024, **358**, 142152.
12. J. Zhuang, N. Rong, X. Wang, C. Chen and Z. Xu, *Separation and Purification Technology*, 2022, **293**, 121133.
13. G. Peng, M. Xiang, W. Wang, Z. Su, H. Liu, Y. Mao, Y. Chen and P. Zhang, *Journal of Hazardous Materials*, 2022, **433**, 128672.
14. T. T. V. Ha, N. M. Viet, P. T. Thanh and V. T. Quan, *Environmental Technology & Innovation*, 2023, **32**, 103265.